Numerical Simulation of Local Weather for a High Photochemical Oxidant Event Using the WRF Model*

Hiroyuki KUSAKA** and Hiroshi HAYAMI***

We evaluated the performance of the newly developed atmospheric mesoscale model, WRF, for the simulation of urban-scale weather in the Tokyo metropolitan area during a high photochemical Oxidant event. The simulation clearly shows that WRF represents the spatial distribution of surface air temperature during the daytime, although the model temperature is lower than the observations in the late afternoon to evening in the urban area. The wind system can be well reproduced in WRF. Simulated convergence zone moves toward the inland areas located to the northwest of the coastal area during the three hours. These results are consistent with the observations of temperature and Photochemical Oxidant, indicating that WRF has enough potential to predict the ongoing Oxidant concentration.

Key Words: Numerical Simulation, Local Weather, Photochemical Oxidant, Mesoscale Meteorological Model, WRF

1. Introduction

Mesoscale meteorological models have been widely used for the analysis and prediction of urban heat island phenomenon(1)–(3) and air quality(3)–(7). The Weather Research and Forecasting (WRF) model(8) is a next-generation mesoscale model with the advanced dynamics, physics, and numerical schemes, and thus it is expected that WRF is more useful than the current community models such as MM5(9) in the analysis and prediction of the urban-scale local weather. Many mesoscale model users will use WRF for simulations of the heat island and air quality in the near future, however the performance of the WRF model for simulation of local weather has yet to be investigated. In the present study, we evaluate the performance of the WRF model for simulation of local weather in the Tokyo metropolitan area (the Kanto area, Fig. 1) during a high photochemical Oxidant event.

2. Description of the Weather Research and Forecasting Model, WRF

The WRF model has been developed via collaboration among the National Center for Atmospheric Research (NCAR), National Center for Environmental Prediction (NCEP), Forecast System Laboratory of the NOAA (NOAA/FSL), and Air Force Weather Agency (AFWA). The WRF model is a compressible, non-hydrostatic, Euler equation, mesoscale meteorological model, and the ARW core version of this model is defined as the next-generation model after MM5, which has been widely used all over the world. One of the strengths of WRF is that the dynamical core uses high-order accurate discretization schemes for time and space(10),(11). Time integration scheme is the third-order Runge-Kutta scheme with smaller time step for

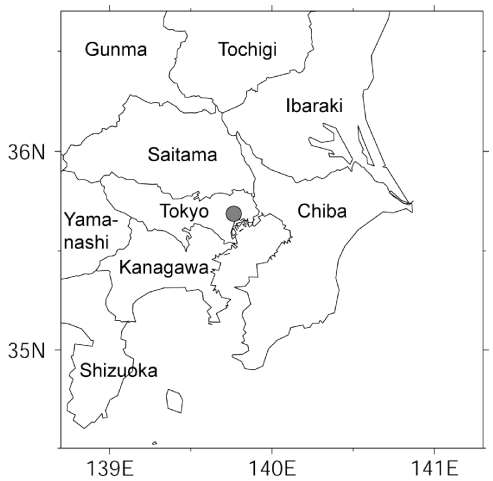

Fig. 1 Map of the Kanto area, including the prefecture and capital city names. Solid line indicates the boundary of the prefectures. A filled circle indicates the urban observation site, Otemachi (35.69N, 139.76E)

* Received 25th November, 2005 (No. 05-4254)

** Fluid Science Sector, Central Research Institute of Electric Power Industry, 1646 Abiko, Abiko, Chiba 270–1194, Japan. E-mail: h-kusaka@criepi.denken.or.jp

*** Environmental Chemistry Sector, Central Research Institute of Electric Power Industry, 1646 Abiko, Abiko, Chiba 270–1194, Japan. E-mail: haya@criepi.denken.or.jp

acoustic and gravity-wave modes. Spatial discretization schemes of the second- to sixth-order accuracy can be selected for the advection terms written in the Arakawa-C grid. Another strength is that the new physics schemes are incorporated.

The model's prognostic variables are horizontal velocity components u and v, vertical velocity w, perturbation potential temperature, perturbation geopotential, perturbation surface pressure, and water vapor mixing ratio; optionally, turbulence kinetic energy and mixing ratio of cloud water, rain water, snow, and ice. The equations are written in the flux form that is used in the terrain-following mass (hydrostatic-pressure) vertical coordinate. Anisotropic transformations, such as a latitude-longitude grid, is accommodated by defining separate map factors for the x and y transformations. Three map projections are supported for real-data simulation: polar stereographic, Lambert-conformal, and Mercator. Curvature and Coriolis terms are included. Realistic simulations require proper specification of the lateral boundary conditions. Periodic, open, or symmetric boundary conditions are available for idealized simulation. Constant pressure is set at the top boundary condition, and gravity wave absorption by diffusion or Rayleigh damping can be used there. The bottom boundary condition is determined by the land surface model. Free-slip is also available for idealized simulations. There are many models for physical processes such as cloud microphysics model, cumulus parameterization, land surface model, surface layer model, boundary layer model, and atmospheric radiation model. Several options are available for each process. Physics (options) used in the present study are described in the Appendix.

3. Numerical Simulation of Local Weather in the Tokyo Metropolitan Area

Figure 2 illustrates surface weather chart at 0900 Japan Standard Time (JST) on July 5 2001. In the early afternoon between 1200 and 1500 JST, the Oxidant concentration was very high (Fig. 3). At 1200 JST, the regions of 80 ppb were spread in and around Tokyo, Saitama, Yamanashi, Shizuoka, and Tochigi prefectures. In particular, the regions with 100 ppb were found in the center of Saitama. By 1500 JST, the regions with 80 ppb were spread in Saitama prefecture, western part of Tochigi prefecture, and Gunma prefecture. We can also confirm the particularly strong concentration over 100 ppb in Gunma prefecture. The high concentration areas moved northwest during the three hours.

Figure 4 shows the spatial distribution of daytime surface air temperature. At 1200 JST, most of the Kanto area was higher than 32.5°C, and the regions with temperature higher than 35°C appeared in northern and western parts of Tokyo and in the western part of Saitama prefecture. By 1500 JST, temperature reached higher than 35°C in the entire Saitama prefecture and a part of the Gunma and Tochigi prefecture. Figure 5 displays the local wind

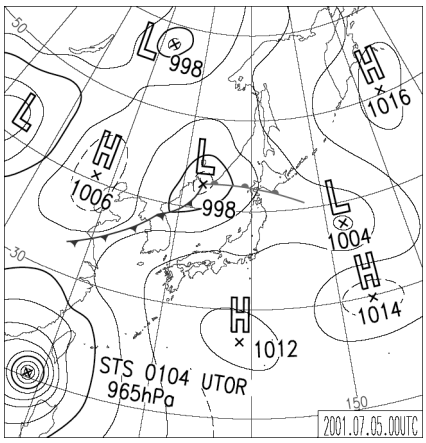

Fig. 2 Surface weather chart on 0900 JST July 5 2001

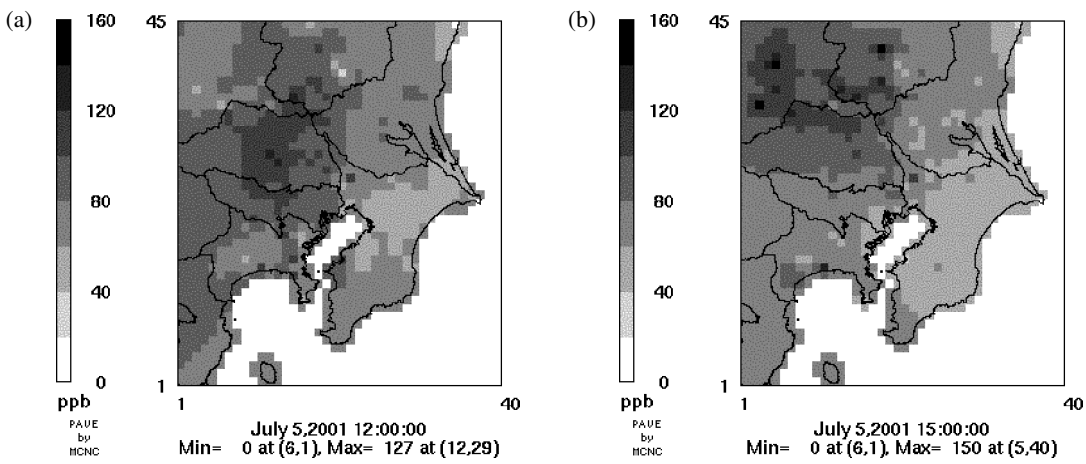

Fig. 3 Observed spatial distribution of the photochemical Oxidant concentration at (a) 1200 JST and (b) 1500 JST on July 5 2001

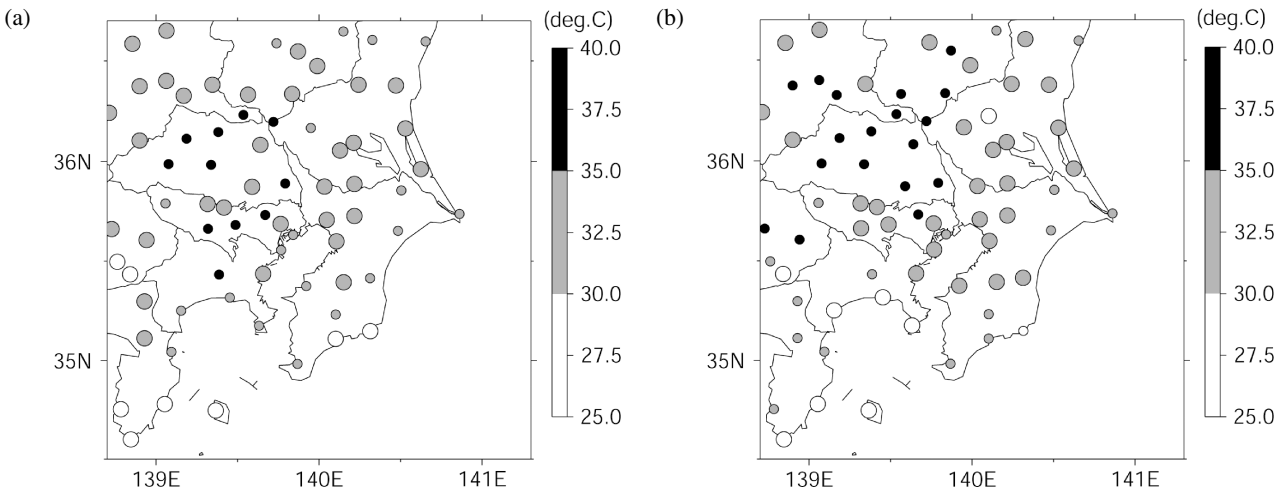

Fig. 4 Observed spatial distribution of the 1.5-m temperature at (a) 1200 JST and (b) 1500 JST on July 5 2001. Larger circles indicate higher temperature if the color is the same

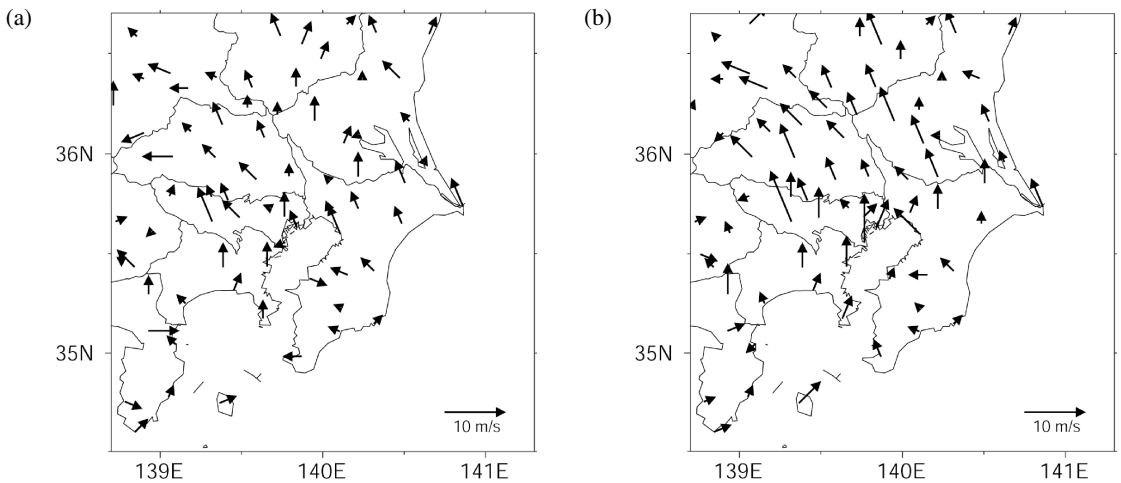

Fig. 5 Observed wind fields at (a) 1200 JST and (b) 1500 JST on July 5 2001. The height of wind measurement is set to be 6 m in most of AMeDAS, but the height in some stations are not precise 6 m

field at 1200 and 1500 JST. At 1200 JST, the southern part of the Kanto area was dominated by southerly and southeasterly winds. The northwestern part of the plain was covered by the southeasterly winds, while southerly winds were predominant in the northeastern part. By 1500 JST, these winds became stronger and southeasterly winds covered the northern part of the plain. This phenomenon is regarded as the so-called 'extended sea breezes', which is generated by the interaction between sea breeze and valley wind.

In the present study, we simulated the local weather during this event using WRF. Model domain is 750 km in the horizontal direction, which includes the Kanto area. The top level is set to be 50 hPa. The initial time of the simulation is 2100 JST on July 4 2001 and the time integration is done for 30 h. JMA-RSM analysis data is employed for creating the initial and boundary conditions. The other configurations are summarized in Table 1.

Table 1 Configuration of the WRF model used in the present study

Numerical and Physical processes	Scheme and Model
Coordinate system	Mass coordinate system
Horizontal advection scheme	5th-order accurate upwind scheme
Vertical advection scheme	3rd-order accurate upwind scheme
Land surface	SLAB (5-layer)
Surface layer	Monin-Obukhov similarity theory
Planetary boundary layer	MRF
Horizontal diffusion	2D-Smagorinsky
Short wave radiation	Dudhia simple
Long wave radiation	RRTM
Cloud microphysics	WSM3
Cumulus parameterization	Not used
Initial and boundary conditions	JMA Regional Spectral Model Analysis Data

Figure 6 is the comparison of the solar radiation between model outputs and observations. The model output agrees with the observations well, although the former slightly overestimates the latter in the morning. Figure 7 shows the spatial distribution of 2-m temperature simulated by WRF. The simulated results roughly agree with the observed ones at both of 1200 and 1500 JST. The diurnal variation is also represented well during the day-

time, although the temperature cooling is more rapid in the model than the observations in the late afternoon to evening at Otemachi that is one of the biggest office areas in Tokyo (Fig. 8). This should be due to the lack of urban canopy processes and anthropogenic heat[(12)–(15)]. The simulated wind field agrees well with the observations at both of 1200 and 1500 JST (Fig. 9). Another important point is that the convergence zone is formed by the sea breezes, and the zone moves toward Gunma prefecture from Saitama prefecture by 1500 JST. These are coherent with the observations of temperature and Photochemical Oxidant that is strongly affected by the advection. The results suggest that the WRF has enough potential to predict the ongoing Oxidant concentration.

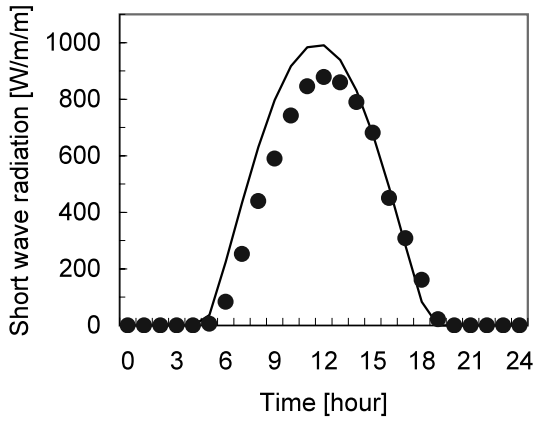

Fig. 6 Time developments of solar radiation in the model output (line) and in the observation (dot) at Otemachi July 5 2001

4. Summary

In this study, we evaluated the performance of the newly developed atmospheric mesoscale model, WRF, for the simulation of local weather in the Tokyo metropolitan area during a high Photochemical Oxidant event.

The simulation clearly shows that WRF represents the spatial distribution of surface air temperature during the daytime. The wind system is also well reproduced in WRF. The simulated convergence zone moves toward Gunma prefecture located to the northwest of Tokyo. These results are consistent with the observations of temperature and Photochemical Oxidant, suggesting that WRF has enough potential to predict the ongoing Oxidant

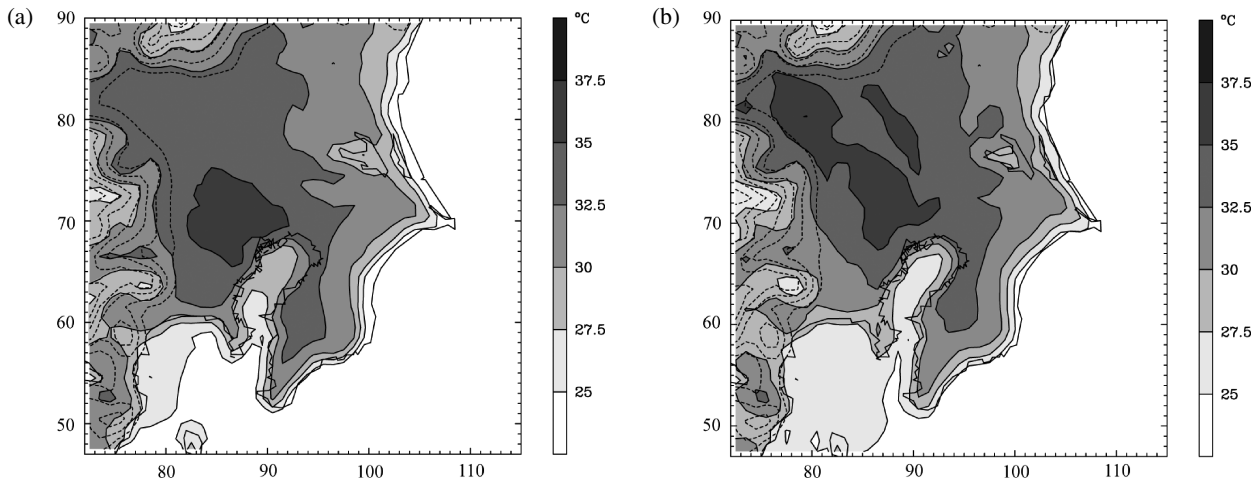

Fig. 7 Simulated spatial distribution of the 2-m temperature at (a) 1200 JST and (b) 1500 JST on July 5 2001. West and south axes are the number of grid point in the WRF model

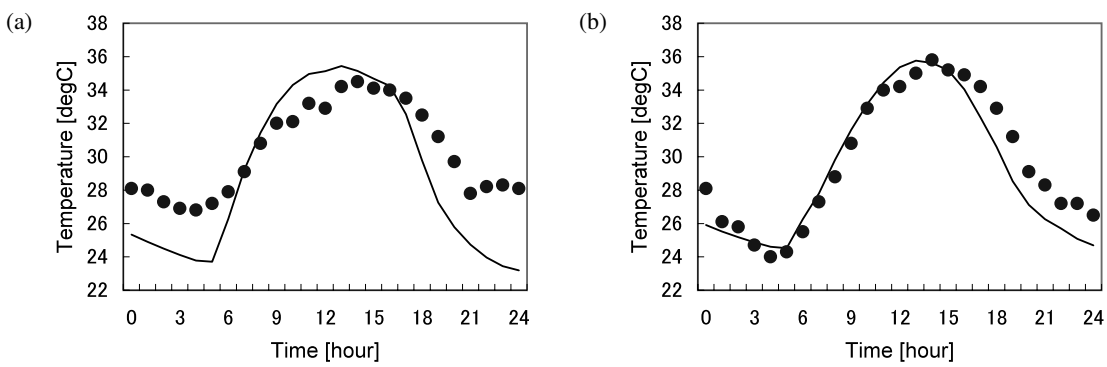

Fig. 8 (to be continued)

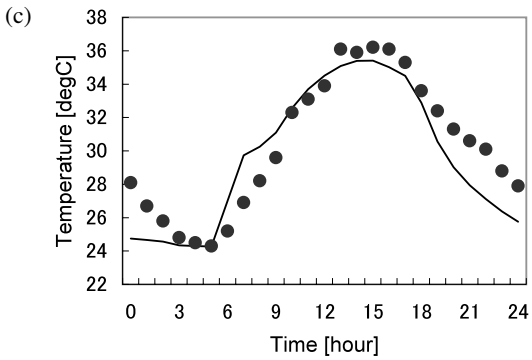

Fig. 8 Diurnal variations of observed (dot) and simulated (line) temperature at (a) Otemachi, (b) Urawa (35.875 N, 139.585E), (c) Maebashi (36.405N, 139.006E)

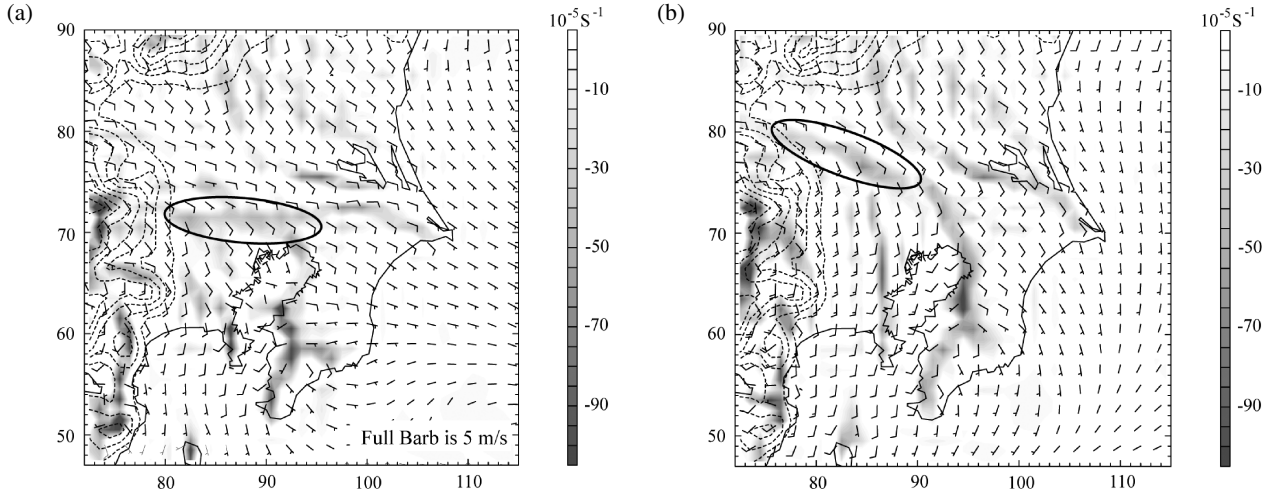

Fig. 9 Simulated 10-m wind fields and convergence zones at (a) 1200 JST and (b) 1500 JST July 5 2001. Shaded areas indicate convergence zones. In both panels above, the oval marked by the solid line indicates the convergence zones. West and south axes are the number of grid point in the WRF model

concentration.

Of course, WRF has some shortcomings. One of them is that WRF has a tendency to estimate the urban temperature to be lower, particularly at night. Therefore, further improvements are required for the land surface processes. In fact, the land surface modeling group in the WRF project is currently trying to embed urban canopy processes in the WRF model. The preliminary results show that the modified WRF well reproduces the nocturnal heat island of Tokyo, whereas the standard one fails the reproduction[16]. The comparison indicates that the urban canopy model can improve the local weather prediction. The mesocale events of Photochemical Oxidants will be simulated by this modified WRF and CMAQ[17] in near future.

Acknowledgment

We thank Dr. Shree Khare of National Center for Atmospheric Research for his comments.

Appendix

(1) WSM3

This scheme predicts three categories of hydrometers: water vapor, cloud/ice, and rain/snow. This is simple and computationally efficient scheme because the cloud ice and cloud water are counted as the same category. They are distinguished by temperature: namely, cloud ice can only exist when the temperature is less than or equal to the freezing point; otherwise, cloud water can exit. The same condition is applied to rain and snow.

(2) SLAB

This scheme calculates surface sensible heat, latent heat, and momentum fluxes using the energy budget equation, and surface and soil temperatures using the heat equation with five-layers. This is simple and computationally efficient scheme because snow cover and soil moisture are fixed and vegetation and urban effects are not explicitly considered. Vegetation and urban effects are considered by tuning surface parameters such as roughness length, albedo, soil moisture, heat capacity and thermal conduc-

tivity.

(3) Similarity theory

This scheme calculates the surface exchange coefficients for heat, moisture, and momentum based on Monin-Obukhov similarity theory. Stability function and length are iteratively calculated.

(4) MRF

This scheme calculates vertical diffusion coefficient with an implicit local scheme. This is non-local scheme and employs a counter-gradient flux for heat and moisture in unstable conditions. This is computationally efficient scheme because there is no prognostic variable such as turbulence kinetic energy.

(5) Dudhia shortwave

This scheme estimates downward integration of solar flux, accounting for clear-air scattering, water vapor absorption, and cloud albedo and absorption. This is computationally efficient because it uses look-up tables for clouds.

(6) RRTM

This scheme estimates atmospheric longwave radiation. This is a spectral-band scheme using the correlated-k method. It uses pre-set tables to accurately represent long-wave processes due to water vapor, ozone, CO_2, and trace gases, as well as accounting for cloud optical depth.

References

(1) Kusaka, H., Kimura, F., Hirakuchi, H. and Mizutori, M., The Effects of Land-Use Alteration on the Sea Breeze and Daytime Heat Island in the Tokyo Metropolitan Area, J. Meteor. Soc. Japan, Vol.78 (2000), pp.405–420.

(2) Kanda, M., Inoue, Y. and Uno, I., Numerical Study on Cloud Lines over an Urban Street in Tokyo, Bound.-Layer Meteor., Vol.98 (2001), pp.251–273.

(3) Ohashi, Y. and Kida, H., Effects of Mountains and Urban Areas on Daytime Local-Circulations in the Osaka and Kyoto Regions, J. Meteor. Soc. Japan, Vol.80 (2002), pp.539–560.

(4) Kimura, F., A Numerical Simulation of Local Winds and Photochemical Air Pollution (II): Application to the Kanto Plain, J. Meteor. Soc. Japan, Vol.63 (1985), pp.923–936.

(5) Kaneyasu, N., Yoshikado, H., Kondo, H., Moriya, T., Suzuki, M. and Shirakawa, Y., Modeling of Suspended Particulate Matter during Early-Winter Severe Pollution Episodes (II): Model Description and the Preliminary Results of Simulation, J. Jpn. Soc. Atmos. Environ., Vol.37 (2002), pp.302–319.

(6) Uno, I., Carmichael, G.R., Streets, D.G., Tang, Y., Yienger, J.J., Satake, S., Wang, Z., Woo, J.-H., Guttikunda, S., Uematsu, M., Matsumoto, K., Tanimoto, H., Yoshida, K. and Iida, T., Regional Chemical Weather Forecasting System CFORS: Model Descriptions and Analysis of Surface Observations at Japanese Island Stations during the ACE-Asia Experiment, J. Geophy. Res., Vol.108 (2003), doi10.1029/2002JD002845.

(7) Otte, T.L., Pouliot, G., Pleim, J.E., Young, J.O., Schere, K.L. and Mathur, R., Linking the Eta Model with the Community Multiscale Air Quality (CMAQ) Modeling System to Build a National Air Quality Forecasting System, Weather and Forecasting, Vol.20 (2005), pp.367–384.

(8) Skamarock, W.C., Klemp, J.B., Dudhia, J., Gill, D.O., Barker, D.M., Wang, W. and Powers, J.G., A Description of the Advanced Research WRF Version 2, NCAR/TN-468+STR, (2005), p.88.

(9) Dudhia, J., A Nonhydrostatic Version of the Penn State/NCAR Mesoscale Model: Validation Tests and Simulation of an Atlantic Cyclone and Cold Front, Mon. Wea. Rev., Vol.121 (1993), pp.1493–1513.

(10) Kusaka, H., Crook, A., Knievel, J.C. and Dudhia, J., Sensitivity of the WRF Model to Advection and Diffusion Schemes for Simulation of Heavy Rainfall along the Baiu Front, SOLA, Vol.1 (2005), pp.177–180.

(11) Kusaka, H., Crook, A., Dudhia, J. and Wada, K., Comparison of the WRF and MM5 Models for Simulation of Heavy Rainfall along the Baiu Front, SOLA, Vol.1 (2005), pp.197–200.

(12) Kusaka, H., Kondo, H., Kikegawa, Y. and Kimura, F., A Simple Single-Layer Urban Canopy Model for Atmospheric Models: Comparison with Multi-Layer and Slab Models, Bound.-Layer Meteor., Vol.101 (2001), pp.329–358.

(13) Kusaka, H. and Kimura, F., Coupling a Single-Layer Urban Canopy Model with a Simple Atmospheric Model: Impact on Urban Heat Island Simulation for an Idealized Case, J. Meteor. Soc. Japan, Vol.82 (2004), pp.67–80.

(14) Kusaka, H. and Kimura, F., Thermal Effects of Urban Canyon Structure on the Nocturnal Heat Island: Numerical Experiment Using Mesoscale Model Coupled with Urban Canopy Model, J. Appl. Meteor., Vol.43 (2004), pp.1899–1910.

(15) Kondo, H., Genchi, Y., Kikegawa, Y., Ohashi, Y., Yoshikado, H. and Komiyama, H., Development of a Multi-Layer Urban Canopy Model for the Analysis of Energy Consumption in a Big City; Structure of the Urban Canopy Model and Its Basic Performance, Bound.-Layer Meteor., Vol.116 (2005), pp.395–421.

(16) Kusaka, H., Chen, F., Tewari, M. and Hirakuchi, H., Impact of the Urban Canopy Model in the Next-Generation Numerical Weather Prediction Model, WRF, Environmental Systems Research, (in Japanese), Vol.33 (2005), pp.159–164.

(17) Byun, D.W. and Ching, J.K.S., Eds., Science Algorithms of the EPS Models-3 Community Multiscale Air Quality (CMAQ) Modeling System, EPA Report N. EPA-600/R-99/030, Office of Research and Development, US Environmental Protection Agency, Washington, D.C., (1999).